Effect of asymmetric concentration profile on thermal conductivity in Ge/SiGe superlattices

Konstanze R. Hahn, Stefano Cecchi, and Luciano Colombo

Articles you may be interested in

Thermal transport in porous Si nanowires from approach-to-equilibrium molecular dynamics calculations
Applied Physics Letters **109**, 013107 (2016); 10.1063/1.4955038

Thermal conductivity of Si–Ge superlattices
Applied Physics Letters **70**, 2957 (1998); 10.1063/1.118755

Thermal conductivity of Si/SiGe and SiGe/SiGe superlattices
Applied Physics Letters **80**, 1737 (2002); 10.1063/1.1455693

Nanoscale thermal transport. II. 2003–2012
Applied Physics Reviews **1**, 011305 (2014); 10.1063/1.4832615

Enhanced thermoelectric figure of merit in nanostructured n-type silicon germanium bulk alloy
Applied Physics Letters **93**, 193121 (2008); 10.1063/1.3027060

Nanoscale thermal transport
Journal of Applied Physics **93**, 793 (2002); 10.1063/1.1524305

Effect of asymmetric concentration profile on thermal conductivity in Ge/SiGe superlattices

Konstanze R. Hahn,[1,a)] Stefano Cecchi,[2] and Luciano Colombo[1,3,4]

[1]*Department of Physics, University of Cagliari, Cittadella Universitaria, 09042 Monserrato (CA), Italy*
[2]*Department of Epitaxy, Paul-Drude-Institut für Festkörperelektronik, Hausvogteiplatz 5-7, 10117 Berlin, Germany*
[3]*Institut de Ciència de Materials de Barcelona (ICMAB-CSIC), Campus UAB, Bellaterra, 08193 Barcelona, Spain*
[4]*Catalan Institute of Nanoscience and Nanotechnology (ICN2), CSIC and The Barcelona Institute of Science and Technology, Campus UAB, Bellaterra, 08193 Barcelona, Spain*

The effect of the chemical composition in Si/Ge-based superlattices on their thermal conductivity has been investigated using molecular dynamics simulations. Simulation cells of Ge/SiGe superlattices have been generated with different concentration profiles such that the Si concentration follows a step-like, a tooth-saw, a Gaussian, and a gamma-type function in direction of the heat flux. The step-like and tooth-saw profiles mimic ideally sharp interfaces, whereas Gaussian and gamma-type profiles are smooth functions imitating atomic diffusion at the interface as obtained experimentally. Symmetry effects have been investigated comparing the symmetric profiles of the step-like and the Gaussian function to the asymmetric profiles of the tooth-saw and the gamma-type function. At longer sample length and similar degree of interdiffusion, the thermal conductivity is found to be lower in asymmetric profiles. Furthermore, it is found that with smooth concentration profiles where atomic diffusion at the interface takes place the thermal conductivity is higher compared to systems with atomically sharp concentration profiles. *Published by AIP Publishing.*
[http://dx.doi.org/10.1063/1.4949491]

A still limiting factor for the large scale use of thermoelectric devices is their comparatively high cost/Watt ratio. It is thus of great interest to optimize the efficiency of the thermoelectric material by maximizing its figure of merit ZT.[1–3] A possible strategy to increase ZT is the introduction of impurities, for example by alloying as indeed observed in $Si_{1-x}Ge_x$ alloys.[4–8]

The reduction of thermal conductivity in alloys is a result of high-frequency phonon scattering at impurity atoms. Alloying however does not affect mid- and low-frequency phonons.[1,2] In order to suppress the propagation of such phonons, it is useful to generate nanofeatures as confirmed by several theoretical and experimental studies.[6,8–12] The decrease of the thermal conductivity κ results from increased phonon scattering at the interfaces introduced by nanograins, nanowires, or superperiodicity.

In the last decades, numerous studies have been dedicated to the investigation of Si/Ge superlattices.[12–20] In particular, it has been shown that diffusion of the counter atoms in Si/Ge superlattices can result in scattering of phonons at all frequencies.[20,21] Recently, Si/SiGe superlattices have been generated experimentally with a graded (tooth-saw) concentration profile providing a lower thermal conductivity with respect to the thermal conductivity in the homogeneous SiGe alloy.[15] However, the effect and interplay of different phonon scattering processes in such superlattice structures is still not well understood.

In this study, we have used molecular dynamics simulations to estimate the thermal conductivity in Ge/SiGe superlattices with different sharp as well as broad concentration profiles that imitate diffusion processes at the interface region. The choice of such a system is inspired by the work of Llin and coauthors,[13] where multilayers of Ge/SiGe have been generated experimentally for industrially applicable thermoelectric devices.

The Ge/SiGe superlattices are oriented with the crystallographic (001) plane orthogonal to the heat flux and are built of several layers of crystalline Ge and a barrier consisting of a SiGe alloy. To account for periodic boundary conditions, the in-plane lattice spacing has been equally set to $a_{Ge,0} = 5.6567\,\text{Å}$ for both Ge and SiGe sections. The out-of-plane lattice parameter has been calculated from the elastic properties of the material as described previously[22] and has been adjusted for each corresponding Si concentration.

One unit block consisting of a Ge and a SiGe alloy section is replicated in z-direction (direction of the heat flux) to generate superlattices. The unit block consists of $n_p = 24$ biatomic layers corresponding to 6.7 nm. The atomic configuration in the unit blocks has been generated according to four different concentration profiles which are based (i) on a step-like function (*step*), (ii) on a Gaussian distribution (*gauss*), (iii) on a gamma-type distribution (*gamma*), and (iv) on a tooth-saw profile (*tooth*). In all samples, the total average Ge concentration is maintained at 83.3%, and the maximum concentration of Si in the SiGe alloy reaches 50% according to recent experimental studies.[13] The unit blocks have been created by random substitution of Ge atoms with Si, where the number of substitutions for each biatomic layer is defined by the corresponding concentration profile.

a)Electronic mail: konstanze.hahn@dsf.unica.it

The concentration profile of the *step* function (Fig. 1(a)) is defined by

$$c_{Si} = \begin{cases} 0 & n_i \leq n_{Ge} \\ 0.5 & n_i > n_{Ge}, \end{cases} \quad (1)$$

where n_i is the index of the biatomic layer and n_{Ge} is the number of biatomic layers corresponding to crystalline Ge; in this case, $n_{Ge} = 16$.

The *gauss* profile (Fig. 1(a)) is described by

$$c_{Si} = \frac{1}{2} \exp \left\{ -\frac{1}{2} \frac{(n_i - \mu)^2}{\sigma^2} \right\}, \quad (2)$$

where μ is the center of the SiGe section, here $\mu = 20$ (number of biatomic layers). In the performed calculations, σ has been set to 3.2 (corresponding to 0.9 nm).

The *gamma* profile (Fig. 1(b)) has been generated based on

$$c_{Si} = \begin{cases} \frac{1}{2} e^{-\frac{1}{2} \cdot n_i} & n_i \leq n_{Ge} \\ \frac{1}{2} \left(1 - e^{-\frac{(n_i - n_{Ge})}{\gamma}} + \frac{1}{n_{SiGe}} e^{-\frac{n_{SiGe}(n_i - n_{Ge})}{\gamma}} \right) & n_i > n_{Ge}, \end{cases} \quad (3)$$

with $n_{Ge} = 16$ and the number of nominal SiGe layers $n_{SiGe} = n_p - n_{Ge} = 8$. The parameter γ has been set to 2.15 (corresponding to 0.6 nm).

The *tooth* profile (Fig. 1(b)) has been generated according to

$$c_{Si} = \begin{cases} 0 & n_i \leq n_{Ge} \\ \frac{0.5}{(n_p - n_{Ge})} \cdot (n_i - n_{Ge}) & n_i > n_{Ge}. \end{cases} \quad (4)$$

In order to obtain a total Ge concentration of 83.3%, the number of crystalline Ge layers is set to $n_{Ge} = 8$.

Molecular dynamics simulations have been performed using the LAMMPS code.[23] Interatomic forces have been described applying the Tersoff pair potential[24] which has been shown to represent reasonably well the mechanical and thermal properties of Si and Ge materials.[8,21,22,25–28] The bond-order Tersoff potential is known to overestimate the frequencies of transverse acoustic modes.[29] This can result in an underestimation of the thermal conductivity at low temperatures (<400 K). Nevertheless, it performs well in predicting lattice thermal conductivity of SiGe alloys in very good agreement with *ab initio* calculations.[8]

Approach-to-equilibrium molecular dynamics (AEMD)[30] have been used to calculate the thermal conductivity following the same protocol already adopted for SiGe heterosystems.[8,31]

The thermal conductivity κ has been estimated in samples with different cell lengths L_z from 200 to 600 nm. The error of the fitted value of κ for all samples presented here is smaller than 0.001 W/mK. It is the standard error of the least squares fit of the simulation data to Fourier's transport equation as used in the AEMD method.[30] In this range, the evolution of the inverse thermal conductivity $1/\kappa$ with the inverse sample length $1/L_z$ follows a linear trend (Fig. 2). The linear relationship between $1/\kappa$ and $1/L_z$ can be expressed according to $\frac{1}{\kappa} = \frac{1}{\kappa_\infty} \left(1 + \frac{\lambda}{L_z} \right)$, where λ is a characteristic length, and
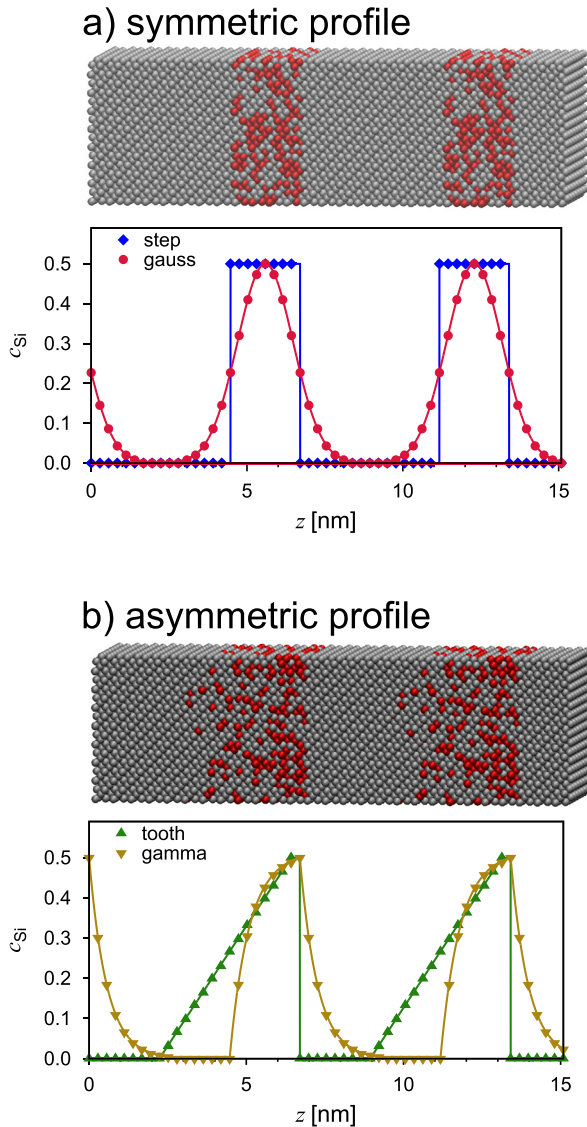

FIG. 1. Section of the simulation cells of the (a) *step* and the (b) *tooth* samples and the corresponding concentration profiles of (a) symmetric and (b) asymmetric samples.
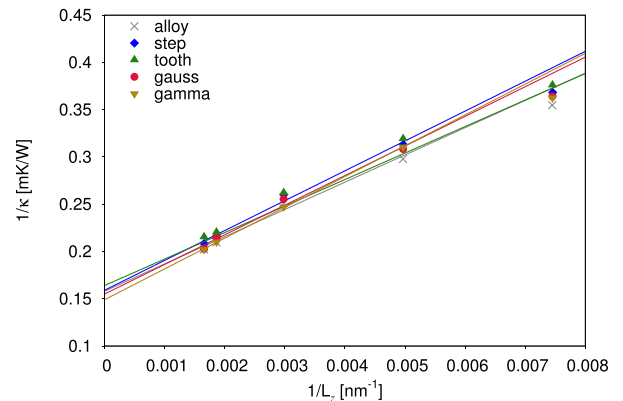

FIG. 2. Inverse thermal conductivity $1/\kappa$ of Ge/SiGe superlattices with different concentration profiles as a function of the inverse simulation cell length $1/L_z$.

it indicates that phonon properties can be estimated well by an average value.[31,32] From the linear trend, the bulk thermal conductivity κ_∞ can be approximated. It is estimated to be between 6.11 (*tooth*) and 6.70 W/mK (*gamma*, Table I).

The thermal conductivity of the atomically sharp concentration profiles *step* (6.29 W/mK) and *tooth* (6.11 W/mK) lies below the value of the homogeneous alloy with the same average Ge concentration of 83.3% (6.34 W/mK). This indicates that in these samples scattering of phonons at the interface, contributing to the thermal boundary resistance in such samples, is more prominent than alloy scattering on impurity atoms in the homogeneous $Si_{0.17}Ge_{0.83}$ sample. On the other hand, when diffusion at the interface takes place, as it is the case for the smooth profiles *gauss* and *gamma*, the thermal conductivity increases to 6.43 and 6.70 W/mK, respectively.

The effect of the sample length on the phonon spectrum has been further analyzed by an accumulation function which represents the fraction of the thermal conductivity that is accumulated with increasing simulation cell length L_z.[31,32] The sample length in this case can be correlated to the mean free path of phonons. Thus, the accumulation function represents the contribution to the thermal conductivity of phonons that have a mean free path smaller than the corresponding sample length L_z. Assuming a normal distribution $f(\Lambda)$ of the mean free path according to $f(\Lambda) = \frac{1}{\sigma\sqrt{2\pi}}\exp\left(-\frac{(\Lambda-\tilde{\mu})^2}{2\sigma^2}\right)$, the accumulation function can be expressed by $\frac{\kappa(\Lambda)}{\kappa_\infty} = \frac{1}{2}\left[1 + \mathrm{erf}\left(\frac{\Lambda-\tilde{\mu}}{\sigma\sqrt{2}}\right)\right]$, where Λ is the logarithm of the dimensionless simulation cell length ($\Lambda = \log\left(\frac{L_z}{\lambda}\right)$) and $\tilde{\mu}$ and σ the mean and the standard deviation, respectively, of the normal distribution of the phonon mean free path. The statistical value $\tilde{\mu}$ can be translated into $\mu = \lambda \cdot 10^{\tilde{\mu}}$ which corresponds to the average value of the phonon mean free path of the system.[31] Fig. 3 shows the accumulation function with the optimized parameters reported in Table I.

In all simulated Ge/SiGe superlattices, the average phonon mean free path is found to be larger (185–208 nm) with respect to the SiGe alloy (176 nm, Table I). This suggests that randomly distributed atomic impurities, as found in the SiGe alloy, lead to a higher reduction of the phonon mean free path than defined interfaces with more pronounced atomic mismatch and is consistent with Garg *et al.*[7] The highest average phonon mean free path is found in the *gamma* sample with 208 nm followed by the one of the *gauss* sample (193 nm). In both profiles, some respective counter
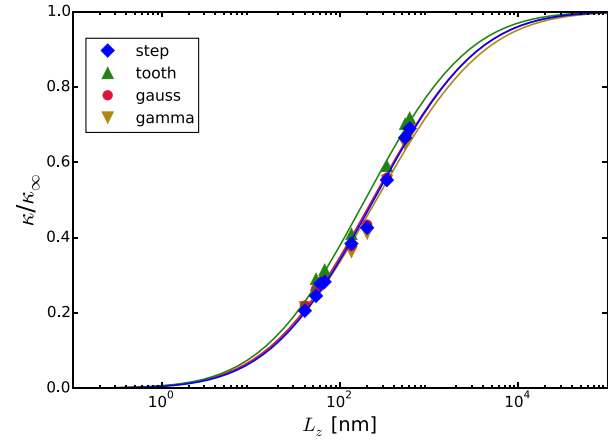

FIG. 3. Accumulation function of the thermal conductivity of Ge/SiGe superlattices with different concentration profiles as a function of the simulation cell length L_z (i.e., mean free path of involved phonons).

atoms diffuse into the other regime at the interface. This generates channels for the phonons to travel through the interfaces which are not atomically sharp as in the *step* and *tooth* profile. In addition, in the *gamma* sample, the region with a Si content <10% is larger than in the *gauss* profile reducing the scattering at impurity atoms which results in a larger phonon mean free path. Assuming a normal distribution of the phonon mean free path, the 68% confidence interval (CI) is similar in all simulated concentration profiles (Table I).

The average Ge content (83.3%) of the simulated superlattices is in the range where the thermal conductivity of the homogeneous alloy is already remarkably decreased compared to the pure Si and Ge.[4–8] Furthermore, the atomic mismatch between the Ge and the $Si_{0.5}Ge_{0.5}$ section is reduced with respect to the mismatch between pure Si and Ge. This results in a very small variation of bulk thermal conductivity with the different concentration profiles simulated here. Approximation of the latter from the linear relationship of $1/\kappa$ to $1/L_z$ is not very precise to accurately capture differences in the thermal transport properties of the different samples. The thermal conductivity has thus been compared directly between the different concentration profiles at three finite simulation cell lengths $L_z = 335$, 537, and 600 nm where the simulations have been run until the rate of time variation of the thermal conductivity resulted to be less than 0.06 W/mK per ns. This typically was observed not before ~4 ns of simulation time for all three cell lengths. Since we are rather interested in relative differences than in absolute values, κ has been normalized to the value of the SiGe alloy at the same cell size. The results are summarized in Fig. 4. The ordering along the horizontal axis follows the increasing asymmetric character of the Si/SiGe interfaces (see Fig. 1).

Independently of the sample length, the thermal conductivity in samples with sharp concentration profiles *step* and *tooth* is lower compared to the smooth profiles *gauss* and *gamma*. At a sample length of $L_z = 335$ and 537 nm, it even reaches higher values than the homogeneous SiGe alloy with the same total Ge concentration of 83.3%. The same is observed for the bulk thermal conductivity κ_∞ (see Table I).

Lower conductivities in the samples with sharp profiles *step* and *tooth* result from enhanced phonon scattering at the interface due to atomic mismatch. Atomic mismatch is

TABLE I. Bulk thermal conductivity for samples with L_z between 200 and 600 nm with the average mean free path μ, obtained from the accumulation function, and the 68% confidential interval (CI) assuming a normal distribution of the phonon mean free path. The goodness of fit of the accumulation function is described by R^2.

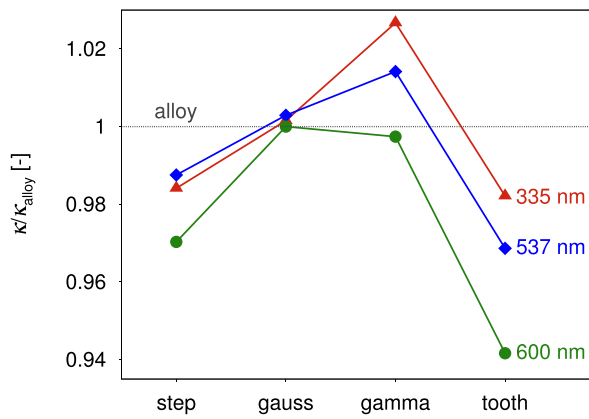| Profile	κ_∞ (W/mK)	μ (nm)	68% CI (nm)	R^2
Alloy	6.34 ± 0.33	176.4 ± 0.02	$33 \div 945$	0.991
Step	6.29 ± 0.29	189.7 ± 0.02	$34 \div 1045$	0.991
Gauss	6.43 ± 0.31	193.0 ± 0.02	$35 \div 1055$	0.990
Gamma	6.70 ± 0.06	207.9 ± 0.01	$37 \div 1171$	0.996
Tooth	6.11 ± 0.16	184.9 ± 0.01	$33 \div 1019$	0.995

FIG. 4. Thermal conductivity of Ge/SiGe superlattices with different concentration profiles estimated at a simulation cell length $L_z = 335$, 537, and 600 nm. Thermal conductivity in systems with sharp interfaces (*step* and *tooth*) is always lower than in systems where interdiffusion at the interface takes place (*gauss* and *gamma*).

reduced when interdiffusion at the interface is present resulting in an increased thermal conductivity in the samples with *gauss* and *gamma* profiles. The present simulation results suggest that in these concentration profiles the thermal boundary resistance is comparatively smaller and thermal transport is mainly affected by alloy scattering at impurity atoms which affects high-frequency phonons.[15,16]

At $L_z = 335$ nm, similar values are found for the thermal conductivity in the *step* and *tooth* profile indicating that the asymmetry has only marginal effect on the thermal transport. This shows that the reduced thermal conductivity with respect to the homogeneous alloy mainly results from interface scattering directed by the atomic mismatch which is the same in the two profiles at the Ge/Si$_{0.5}$Ge$_{0.5}$ interface.

Increasing the sample length, however, leads to a sizable reduction of the thermal conductivity in samples with asymmetric profiles *tooth* and *gamma* with respect to the alloy and the symmetric profiles *step* and *tooth*. The larger is the sample length, the higher is the number of interfaces (i.e., active scattering centers) that a phonon mode must pass through. This reflects in an overall decrease of the (normalized) thermal conductivity. Fig. 4 clearly suggests that asymmetric profiles affect thermal conduction to a considerably larger extent than symmetric ones. This is likely due to a reduction of the correspondent tunneling probability of incoming phonons. As a matter of fact, asymmetric profiles have the same height of their symmetric counterparts, while showing a larger width. This is especially true for the *tooth* profile which, in fact, corresponds to the comparatively smaller conductivity. These findings are in agreement with experimental evidence in samples where gradients in the concentration profiles resulted in a lower thermal conductivity compared to conventional symmetric Ge/SiGe superlattices.[15] Previously, *ab initio* calculations have been used to proof experimental evidence that in Si/Ge superlattices segregation of Ge in the Si layer leads to a decrease of the thermal conductivity with respect to an atomically sharp interface.[20] This type of segregation results in an asymmetric concentration profile which can be compared to the *tooth* profile simulated here. The results shown here are thus in agreement with the latter study showing a lower thermal conductivity of the *tooth* profile with respect to the *step*

profile at a sufficiently large sample length ($L_z > 500$ nm). A direct comparison of the two studies, however, is critical, since there the superlattice layers consisted of pure Si and Ge, respectively, whereas here we simulated boundaries between Ge and the SiGe alloy.

In conclusion, we have shown that the interface diffusion leads to an increase of the thermal conductivity with respect to sharp Ge/SiGe boundaries. At sufficiently long length ($L_z = 600$ nm), the thermal conductivity in systems with asymmetric concentration profiles is lower than for symmetric profiles with comparable interdiffusion at the interface. This effect is attributed to possible tunneling of phonons through the interface as a result of the symmetric composition around the interface. These findings give interesting insight into the effect of concentration profiles on the thermal conductivity in Ge/SiGe superlattices which are hard to be observed experimentally due to small variations in the absolute values. The small changes in heat transport properties predicted by our calculations suggest that for systems similar to the ones investigated here the actual concentration profile only plays a marginal role in affecting the thermal conductivity and, in turn, indicates that the level of accuracy in the present state-of-the-art fabrication of such superlattices is sufficient to generate materials with desired heat transport properties. Nevertheless, the results of this study are a basis for an extended exploration of the thermal transport properties of such Si/Ge-based superlattices as a function of their composition, interface properties, and device dimension.

[1]M. S. Dresselhaus, G. Chen, M. Y. Tang, R. G. Yang, H. Lee, D. Z. Wang, Z. F. Ren, J. P. Fleurial, and P. Gogna, Adv. Mater. **19**, 1043 (2007).
[2]A. J. Minnich, M. S. Dresselhaus, Z. F. Ren, and G. Chen, Energy Environ. Sci. **2**, 466 (2009).
[3]J. Karni, Nat. Mater. **10**, 481 (2011).
[4]H. Stöhr and W. Klemm, Z. Anorg. Allg. Chem. **241**, 305 (1939).
[5]B. Abeles, Phys. Rev. **131**, 1906 (1963).
[6]X. W. Wang, H. Lee, Y. C. Lan, G. H. Zhu, G. Joshi, D. Z. Wang, J. Yang, A. J. Muto, M. Y. Tang, J. Klatsky, S. Song, M. S. Dresselhaus, G. Chen, and Z. F. Ren, Appl. Phys. Lett. **93**, 193121 (2008).
[7]J. Garg, N. Bonini, B. Kozinsky, and N. Marzari, Phys. Rev. Lett. **106**, 045901 (2011).
[8]C. Melis and L. Colombo, Phys. Rev. Lett. **112**, 065901 (2014).
[9]S. K. Bux, R. G. Blair, P. K. Gogna, H. Lee, G. Chen, M. S. Dresselhaus, R. B. Kaner, and J.-P. Fleurial, Adv. Funct. Mater. **19**, 2445 (2009).
[10]Y. P. He, D. Donadio, and G. Galli, Nano Lett. **11**, 3608 (2011).
[11]S. Bathula, M. Jayasimhadri, N. Singh, A. K. Srivastava, J. Pulikkotil, A. Dhar, and R. C. Budhani, Appl. Phys. Lett. **101**, 213902 (2012).
[12]I. Savić, D. Donadio, F. Gygi, and G. Galli, Appl. Phys. Lett. **102**, 073113 (2013).
[13]L. F. Llin, A. Samarelli, S. Cecchi, T. Etzelstorfer, E. M. Gubler, D. Chrastina, G. Isella, J. Stangl, J. M. R. Weaver, P. S. Dobson, and D. J. Paul, Appl. Phys. Lett. **103**, 143507 (2013).
[14]E. Landry and A. McGaughey, Phys. Rev. B **79**, 075316 (2009).
[15]P. Ferrando-Villalba, A. F. Lopeandía, F. X. Alvarez, B. Paul, C. de Tomás, M. I. Alonso, M. Garriga, A. R. Goñi, J. Santiso, G. Garcia, and J. Rodriguez-Viejo, Nano Res. **8**, 2833 (2015).
[16]P. Chen, T. Etzelstorfer, F. Hackl, N. A. Katcho, H.-T. Chang, L. Nausner, S.-W. Lee, T. Fromherz, J. Stangl, O. G. Schmidt, N. Mingo, and A. Rastelli, Phys. Status Solidi A **213**, 533 (2016).
[17]S.-M. Lee, D. G. Cahill, and R. Venkatasubramanian, Appl. Phys. Lett. **70**, 2957 (1997).
[18]S. T. Huxtable, A. R. Abramson, C.-L. Tien, A. Majumdar, C. LaBounty, X. Fan, G. Zeng, J. E. Bowers, A. Shakouri, and E. T. Croke, Appl. Phys. Lett. **80**, 1737 (2002).
[19]G. Pernot, M. Stoffel, I. Savic, F. Pezzoli, P. Chen, G. Savelli, A. Jacquot, J. Schumann, U. Denker, I. Monch, C. Deneke, O. G. Schmidt, J. M.

Rampnoux, S. Wang, M. Plissonnier, A. Rastelli, S. Dilhaire, and N. Mingo, Nat. Mater. **9**, 491 (2010).

[20]P. Chen, N. A. Katcho, J. P. Feser, W. Li, M. Glaser, O. G. Schmidt, D. G. Cahill, N. Mingo, and A. Rastelli, Phys. Rev. Lett. **111**, 115901 (2013).

[21]R. Dettori, C. Melis, and L. Colombo, Eur. Phys. J. B **88**, 27 (2015).

[22]K. R. Hahn, M. Puligheddu, and L. Colombo, Phys. Rev. B **91**, 195313 (2015).

[23]S. Plimpton, J. Comput. Phys. **117**, 1 (1995).

[24]J. Tersoff, Phys. Rev. B **39**, 5566 (1989).

[25]S. Cook and P. Clancy, Phys. Rev. B **47**, 7686 (1993).

[26]L. J. Porter, S. Yip, M. Yamaguchi, H. Kaburaki, and M. Tang, J. Appl. Phys. **81**, 96 (1997).

[27]X. Li and R. Yang, Phys. Rev. B **86**, 054305 (2012).

[28]X. Li and R. Yang, J. Phys.: Condens. Matter **24**, 155302 (2012).

[29]L. J. Porter, J. F. Justo, and S. Yip, J. Appl. Phys. **82**, 5378 (1997).

[30]C. Melis, R. Dettori, S. Vandermeulen, and L. Colombo, Eur. Phys. J. B **87**, 96 (2014).

[31]K. R. Hahn, C. Melis, and L. Colombo, Eur. Phys. J. B **87**, 150 (2014).

[32]D. P. Sellan, E. S. Landry, J. E. Turney, A. J. H. McGaughey, and C. H. Amon, Phys. Rev. B **81**, 214305 (2010).